IAEA nuclear fusion

PAPER • OPEN ACCESS

Experimental research on the TCV tokamak

To cite this article: B.P. Duval *et al* 2024 *Nucl. Fusion* **64** 112023

View the article online for updates and enhancements.

You may also like

- Observation of nonthermal electrons further acceleration and long-lasting associated with magnetic reconnection and turbulence bursting in tokamak plasma
  Chaowei Mai, Liqing Xu, Shiyao Lin et al.
- Density fluctuation statistics and turbulence spreading at the edge of L–mode plasmas
  F.O. Khabanov, R. Hong, P. H. Diamond et al.
- Transport and confinement physics: Chapter 2 of the special issue: on the path to tokamak burning plasma operation
  M. Yoshida, R.M. McDermott, C. Angioni et al.


ARE YOU STRUGGLING TO SOURCE MATERIALS?

FIND OUT HOW GOODFELLOW IS HELPING LEAD THE WAY IN MATERIALS RESEARCH

We are proud to support fusion research, supplying materials for groundbreaking advancements since 1946. These include the 2022 LLNL achievement at the National Ignition Facility (NIF). This historic experiment marked the first-ever controlled fusion ignition, producing more energy from the reaction than was used to initiate it.

Click here to find out more about this story.

SEM image showing Fatigue Striations of a Metal

Fully equipped **accredited research laboratory** to conduct in depth analysis of materials.

Supported by experienced team of materials scientists.

Research and industrial scale production for **new materials** and developing **new capabilities.**

We're excited to partner with you to help drive your research forward. Talk to us today.

goodfellow
ADVANCED MATERIALS

EXPLORE OUR FULL RANGE OF IN STOCK MATERIALS.

- LITHIUM
- TUNGSTEN
- PALLADIUM SILVER ALLOYS AND MUCH MORE

SCAN THE QR CODE HERE OR VISIT:
goodfellow.com/nuclearfusionjournal

This content was downloaded from IP address 87.0.77.133 on 25/03/2025 at 11:26

OPEN ACCESS
IOP Publishing | International Atomic Energy Agency
Nuclear Fusion
Nucl. Fusion **64** (2024) 112023 (15pp)
https://doi.org/10.1088/1741-4326/ad8361

Experimental research on the TCV tokamak

**B.P. Duval[1,*], A. Abdolmaleki[2], M. Agostini[3], C.J. Ajay[4], S. Alberti[1], E. Alessi[5],
G. Anastasiou[6], Y. Andrèbe[1], G.M. Apruzzese[7], F. Auriemma[3], J. Ayllon-Guerola[8],
F. Bagnato[1], A. Baillod[1], F. Bairaktaris[9], L. Balbinot[3], A. Balestri[1], M. Baquero-Ruiz[1],
C. Barcellona[10], M. Bernert[11], W. Bin[5], P. Blanchard[1], J. Boedo[12], T. Bolzonella[3],
F. Bombarda[7], L. Boncagni[7], M. Bonotto[3], T.O.S.J. Bosman[13,43], D. Brida[11], D. Brunetti[14],
J. Buchli[2], J. Buerman, P. Buratti[16], A. Burckhart[11], D. Busil[17], J. Caloud[18], Y. Camenen[19],
A. Cardinali[7], S. Carli[20], D. Carnevale[16], F. Carpanese[1,2], M. Carpita[1], C. Castaldo[7],
F. Causa[5], J. Cavalier[18], M. Cavedon[21], J.A. Cazabonne[1], J. Cerovsky[18], B. Chapman[14],
M. Chernyshova[22], P. Chmielewski[22], A. Chomiczewska[22], G. Ciraolo[23], S. Coda[1],
C. Colandrea[1], C. Contré[1], R. Coosemans[1], L. Cordaro[3], S. Costea[24], T. Craciunescu[25],
K. Crombe[15,48], A. Dal Molin[5], O. D'Arcangelo[7,26], D. de Las Casas[2], J. Decker[1],
J. Degrave[2], H. de Oliveira[1], G.L. Derks[13,43], L.E. di Grazia[26,49], C. Donner[2], M. Dreval[27],
M.G. Dunne[11], G. Durr-Legoupil-Nicoud[1], B. Esposito[7], T. Ewalds[2], M. Faitsch[11],
M. Farník[18], A. Fasoli[1], F. Felici[1], J. Ferreira[28], O. Février[1], O. Ficker[18], A. Frank[1],
E. Fransson[29], L. Frassinetti[30], L. Fritz[2], I. Furno[1], D. Galassi[1], K. Gałązka[22,23],
J. Galdon-Quiroga[8], S. Galeani[16], C. Galperti[1], S. Garavaglia[5], M. Garcia-Munoz[8],
P. Gaudio[16], M. Gelfusa[16], J. Genoud[1], R. Gerrú Miguelanez[31], G. Ghillardi[7], M. Giacomin[1],
L. Gil[28], A. Gillgren[29], C. Giroud[14], T. Golfinopoulos[32], T. Goodman[1], G. Gorini[2,15],
S. Gorno[1], G. Grenfell[11], M. Griener[11], M. Gruca[22], T. Gyergyek[24], R. Hafner[2], M. Hamed[13],
D. Hamm[1], W. Han[32], G. Harrer[33], J.R. Harrison[14], D. Hassabis[2], S. Henderson[14],
P. Hennequin[34], J. Hidalgo-Salaverri[8], J-P. Hogge[1], M. Hoppe[1,30], J. Horacek[18], A. Huber[2],
E. Huett[1], A. Iantchenko[1], P. Innocente[3], C. Ionita-Schrittwieser[35], I. Ivanova Stanik[22],
M. Jablczynska[22], A. Jansen van Vuuren[8], A. Jardin[36], H. Järleblad[31], A.E. Järvinen[37],
J. Kalis[11], R. Karimov[1], A.N. Karpushov[1], K. Kavukcuoglu[2], J. Kay[2], Y. Kazakov[15],
J. Keeling[2], A. Kirjasuo[38], J.T.W. Koenders[13,43], P. Kohli[2], M. Komm[18], M. Kong[1,14],
J. Kovacic[24,50], E. Kowalska-Strzeciwilk[22], O. Krutkin[1], O. Kudlacek[11], U. Kumar[1],
R. Kwiatkowski[39], B. Labit[1], L. Laguardia[5], E. Laszynska[22], A. Lazaros[9], K. Lee[1],
E. Lerche[15], B. Linehan[32], D. Liuzza[7], T. Lunt[11], E. Macusova[18], D. Mancini[1,40], P. Mantica[5],
M. Maraschek[11], G. Marceca[1], S. Marchioni[1], A. Mariani[5], M. Marin[1], A. Marinoni[32],
L. Martellucci[16], Y. Martin[1], P. Martin[3], L. Martinelli[1], F. Martinelli[16], J.R. Martin-Solis[41],
S. Masillo[1], R. Masocco[16], V. Masson[1], A. Mathews[1], M. Mattei[26], D. Mazon[23], S. Mazzi[1,23],
S. Mazzi[1], S.Y. Medvedev[42], C. Meineri[3], A. Mele[26], V. Menkovski[43], A. Merle[1], H. Meyer[14],
K. Mikszuta-Michalik[22], I.G. Miron[25], P.A. Molina Cabrera[1], A. Moro[5], A. Murari[3,51],
P. Muscente[3,52], D. Mykytchuk[1], F. Nabais[28], F. Napoli[7], R.D. Nem[31], M. Neunert[2],
S.K. Nielsen[31], A. Nielsen[31], M. Nocente[21], S. Noury[2], S. Nowak[5], H. Nyström[30],
N. Offeddu[1], S. Olasz[44], F. Oliva[16], D.S. Oliveira[1], F.P. Orsitto[26], N. Osborne[45],
P. Oyola Dominguez[8], O. Pan[11], E. Panontin[21], A.D. Papadopoulos[9], P. Papagiannis[9],
G. Papp[11], M. Passoni[17], F. Pastore[1], A. Pau[1], R.O. Pavlichenko[27], A.C. Pedersen[31],
M. Pedrini[1], G. Pelka[22], E. Peluso[16], A. Perek[1,13], C. Perez Von Thun[22], F. Pesamosca[1],**

---

[*] Author to whom any correspondence should be addressed.

1741-4326/24/112023+15$33.00 Printed in the UK

D. Pfau[2], V. Piergotti[7], L. Pigatto[3], C. Piron[7], L. Piron[3,52], A. Pironti[26], U. Plank[11], V. Plyusnin[28], Y.R.J. Poels[1,43], G.I. Pokol[44], J. Poley-Sanjuan[1], M. Poradzinski[22], L. Porte[1], C. Possieri[16], A. Poulsen[31], M.J. Pueschel[13,43], T. Pütterich[11], V. Quadri[23], M. Rabinski[39], R. Ragona[31], H. Raj[1], A. Redl[40], H. Reimerdes[1], C. Reux[23], D. Ricci[5], M. Riedmiller[2], S. Rienäcker[34], D. Rigamonti[5], N. Rispoli[5], J.F. Rivero-Rodriguez[14], C.F. Romero Madrid[8], J. Rueda Rueda[8], P.J. Ryan[14], M. Salewski[31], A. Salmi[38], M. Sassano[16], O. Sauter[1], N. Schoonheere[23], R.W. Schrittwieser[35], F. Sciortino[11], A. Selce[5], L. Senni[7], S. Sharapov[14], U.A. Sheikh[1], B. Sieglin[11], M. Silva[1], D. Silvagni[11], B. Simmendefeldt Schmidt[31], L. Simons[1], E.R. Solano[46], C. Sozzi[5], M. Spolaore[3], L. Spolladore[16], A. Stagni[3,52], P. Strand[29], G. Sun[1], W. Suttrop[11], J. Svoboda[18], B. Tal[11], T. Tala[38], P. Tamain[23], M. Tardocchi[5], A. Tema Biwole[1], A. Tenaglia[16], D. Terranova[3,51], D. Testa[1], C. Theiler[1], A. Thornton[14], A.S. Thrysoe[31], M. Tomes[18], E. Tonello[1,17], H. Torreblanca[1], B. Tracey[2], M. Tsimpoukelli[2], C. Tsironis[9], C.K. Tsui[1,12], M. Ugoletti[3], M. Vallar[1], M. van Berkel[13], S. van Mulders[1,53], M. van Rossem[1], C. Venturini[1], M. Veranda[3,51], T. Verdier[31], K. Verhaegh[14], L. Vermare[34], N. Vianello[3,51], E. Viezzer[8], F. Villone[26], B. Vincent[1], P. Vincenzi[3], I. Voitsekhovitch[14], L. Votta[17], N.M.T. Vu[1,53], Y. Wang[1], E. Wang[47], T. Wauters[15], M. Weiland[11], H. Weisen[1], N. Wendler[22], S. Wiesen[47], M. Wiesenberger[31], T. Wijkamp[13,43], C. Wüthrich[1], D. Yadykin[29], H. Yang[23], V. Yanovskiy[18], J. Zebrowski[39], P. Zestanakis[6], M. Zuin[3,51] and M. Zurita[1]

[1] École Polytechnique Fédérale de Lausanne (EPFL), Swiss Plasma Center (SPC), Lausanne, Switzerland
[2] Google DeepMind, London, Ireland
[3] Consorzio RFX, Padova, Italy
[4] York Plasma Institute, University of York, Heslington, York, Ireland
[5] Istituto per la Scienza e Tecnologia dei Plasmi ISTP-CNR, Milano, Italy
[6] Aristotle University of Thessaloniki, Thessaloniki, Greece
[7] Unità Tecnica Fusione, ENEA, Frascati, Italy
[8] Universidad de Sevilla, Sevilla, Spain
[9] Department of Physics, National and Kapodistrian University of Athens, Athens, Greece
[10] Università degli Studi di Catania, Catania, Italy
[11] Max Planck Institute for Plasma Physics, Garching, Germany
[12] Center for Energy Research (CER), University of California-San Diego (UCSD), La Jolla, CA, United States of America
[13] DIFFER-Dutch Institute for Fundamental Energy Research, Eindhoven, Netherlands
[14] CCFE, Culham Science Centre, Abingdon, Oxon, Ireland
[15] Laboratory for Plasma Physics, LPP-ERM/KMS, Brussels, Belgium
[16] University of Rome Tor Vergata, Rome, Italy
[17] Politecnico di Milano, Milan, Italy
[18] Institute of Plasma Physics of the CAS, Prague, Czech Republic
[19] Aix-Marseille Université, CNRS, Marseille, France
[20] Department of Mechanical Engineering, KU Leuven, Leuven, Belgium
[21] Universita' di Milano-Bicocca, Milano, Italy
[22] Institute of Plasma Physics and Laser Microfusion (IPPLM), Warsaw, Poland
[23] CEA, IRFM, Saint Paul-Lez-Durance Cedex, France
[24] Jožef Stefan Institute, Ljubljana, Slovenia
[25] National Institute for Laser, Plasma and Radiation Physics, Magurele, Romania
[26] Università degli Studi di Napoli 'Federico II', Consorzio CREATE, Napoli, Italy
[27] Institute of Plasma Physics of the NSC KIPT, Kharkov, Ukraine
[28] Instituto de Plasmas e Fusão Nuclear, Instituto Superior Técnico, Lisboa, Portugal
[29] Chalmers University of Technology, Gothenburg, Sweden
[30] KTH Royal Institute of Technology, Stockholm, Sweden
[31] Department of Physics, Technical University of Denmark, Kgs, Lyngby, Denmark
[32] Plasma Science and Fusion Center, Massachusetts Institute of Technology, Cambridge, MA, United States of America
[33] Institute of Applied Physics, Fusion at ÖAW, T.U. Wien, Vienna, Austria
[34] Laboratoire des Physique des Plasmas (LPP), Ecole polytechnique, Palaiseau, France
[35] Institut für Ionenphysik und Angewandte Physik, Universität Innsbruck, Innsbruck, Austria
[36] Institute of Nuclear Physics Polish Academy of Sciences (IFJ PAN), Krakow, Poland
[37] Aalto University, Aalto, Finland
[38] VTT, Espoo, Finland

[39] National Centre for Nuclear Research (NCBJ), Otwock, Poland
[40] Department of Economics, Engineering, Society and Business Organization (DEIm), University of Tuscia, Viterbo, Italy
[41] Universidad Carlos III de Madrid, Madrid, Spain
[42] Tokamak Energy, Abingdon, Ireland
[43] Eindhoven University of Technology, Eindhoven, Netherlands
[44] Centre for Energy Research, Budapest, Hungary
[45] University of Liverpool, Liverpool, Ireland
[46] Laboratorio Nacional de Fusión, CIEMAT, Madrid, Spain
[47] Forschungszentrum Jülich GmbH, Institut für Energie- und Klimaforschung—Plasmaphysik, Jülich, Germany
[48] Universiteit Gent, Ghent, Belgium
[49] Università degli Studi della Campania 'L. Vanvitelli', Aversa, Italy
[50] University of Ljubljana, Lyubljana, Slovenia
[51] Istituto per la Scienza e Tecnologia dei Plasmi ISTP-CNR, Padova, Italy
[52] Università degli Studi di Padova, Padova, Italy
[53] ITER Organization, Saint-Paul-lez-Durance, France

E-mail: basil.duval@epfl.ch

Received 25 July 2024, revised 2 September 2024
Accepted for publication 4 October 2024
Published 29 October 2024

Abstract

Tokamak à configuration variable (TCV), recently celebrating 30 years of near-continual operation, continues in its missions to advance outstanding key physics and operational scenario issues for ITER and the design of future power plants such as DEMO. The main machine heating systems and operational changes are first described. Then follow five sections: *plasma scenarios.* ITER Base-Line (IBL) discharges, triangularity studies together with X3 heating and N2 seeding. Edge localised mode suppression, with a high radiation region near the X-point is reported with N_2 injection with and without divertor baffles in a snowflake configuration. Negative triangularity (NT) discharges attained record, albeit transient, $\beta_N \sim 3$ with lower turbulence, higher low-Z impurity transport, vertical stability and density limits and core transport better than the IBL. Positive triangularity L-Mode linear and saturated ohmic confinement confinement saturation, often-correlated with intrinsic toroidal rotation reversals, was probed for D, H and He working gases. H-mode confinement and pedestal studies were extended to low collisionality with electron cyclotron heating obtaining steady state electron iternal transport barrier with neutral beam heating (NBH), and NBH driven H-mode configurations with off-axis co-electron cyclotron current drive. *Fast particle physics.* The physics of disruptions, runaway electrons and fast ions (FIs) was developed using near-full current conversion at disruption with recombination thresholds characterised for impurity species (Ne, Ar, Kr). Different flushing gases (D2, H2) and pathways to trigger a benign disruption were explored. The 55 kV NBH II generated a rich Alfvénic spectrum modulating the FI fas ion loss detector signal. NT configurations showed less toroidal Alfvén excitation activity preferentially affecting higher FI pitch angles. *Scrape-off layer and edge physics.* gas puff imaging systems characterised turbulent plasma ejection for several advanced divertor configurations, including NT. Combined diagnostic array divertor state analysis in detachment conditions was compared to modelling revealing an importance for molecular processes. *Divertor physics.* Internal gas baffles diversified to include shorter/longer structures on the high and/or low field side to probe compressive efficiency. Divertor studies concentrated upon mitigating target power, facilitating detachment and increasing the radiated power fraction employing alternative divertor geometries, optimised X-point radiator regimes and long-legged configurations. Smaller-than-expected improvements with total flux expansion were better modelled when including parallel flows. Peak outer target heat flux reduction was achieved (>50%) for high flux-expansion geometries, maintaining core performance ($H_{98} > 1$). A reduction in target heat loads and facilitated detachment access at lower core densities is reported. *Real-time control.* TCV's real-time control upgrades employed MIMO gas injector control of stable, robust, partial detachment and plasma β feedback control avoiding neoclassical tearing modes with plasma confinement changes. Machine-learning enhancements include trajectory tracking disruption proximity and avoidance as well as a first-of-its-kind reinforcement learning-based controller for the plasma equilibrium trained entirely on a free-boundary simulator. Finally, a short description of TCV's immediate future plans will be given.

Keywords: TCV, review, plasma, SPC, EPFL

(Some figures may appear in colour only in the online journal)

1. Introduction

Tokamak à configuration variable (TCV), is a conventional aspect ratio (R/a = 0.88 m/0.25 m $\sim$ 3.5, $Ip \leqslant 1$ MA, $B\phi \leqslant 1.5$ T, inductive pulse length $\leqslant\sim$2.5 s) medium-sized Tokamak selected for operation within the EUROfusion group [1]. It features strong poloidal shaping options, powerful auxiliary heating sources, a complex control system and an ever-widening range of modern core and divertor diagnostics. The open vacuum vessel walls, protected (>85%) by carbon tiles, have been augmented by a range of interchangeable, internal, gas-flow restriction tiles, called baffles, that are designed such that both the toroidal magnetic field and plasma current directions may still be selected independently for each plasma discharge. Vacuum ports, in the lower machine where most divertor leg configurations are directed, are further protected by tiles that shadow those ports from those divertor legs. This permits nearly all plasma core and divertor configurations to be operated, including high power auxiliary heating, without restriction. TCV's mission is to use its flexibility to help solve outstanding plasma physics and operational issues on the road to Fusion capable devices such as ITER and reactor designs such as DEMO [2]. Over the 2021–2022 campaigns, electron cyclotron heating (ECH) auxiliary heating now includes 1.4 MW 2x83GHz (X2) and 0.9 MW 2x118GHz gyrotrons (X3) and 2x1MW dual frequency (84/126 GHZ) gyrotrons for X2/X3 heating through 6 independent, RT-controlled, launchers. A second, RT-steering capable, vertical launcher and new, validated, in-vessel focusing mirrors, ~180° toroidally apart (X3), complement legacy lateral launchers. A further dual frequency unit is being procured for increased core heating at higher plasma densities. TCV's, 26 kV 1.3 MW, tangential, positive-ion neutral beam was complemented by a 60 kV, 1 MW, counter-tangential beam that delivered up to 1 MJ through a redesigned beam-duct with both injectors H and D compatible. The increase in beam-plasma, fusion resultant, neutron and gamma rates necessitated a complete revision of TCV's radiation shielding. A combination of ~0.5 m of polyethylene and 0.5–1 m of Baryted concrete walls, together with a 0.5 m polyethylene roof over TCV was installed in the first half of 2023, following extensive modelling of neutron and gamma radiation propagation, that has resulted in nearly undetectable external radiation levels now achievable for all TCV operational scenarios [3]. Recently, the celebration of 30 years of near continuous TCV operations was accompanied by a thorough revision of the poloidal coil support systems and the motor generator that powers TCV's discharges and its auxiliary heating systems.

The TCV experimental programmes are executed by topical teams, under the auspices of the EUROfusion Tokamak Exploitation Work Package programme, complemented and often enhanced by local programme teams at the Swiss Plasma Center together with international collaborators. TCV is designed and maintained to operated full discharges (up to 2.5 s inductively) every 10–15 min for many days a week and many days a year. Its signature shaping capabilities, abundant auxiliary heating combinations and rich diagnostic set result in a widely varying range of experimental goals that this, of necessity, relatively short résumé cannot hope to cover in great detail. Care is taken, where possible, to cite the more recent publications where many more of TCV's long publication history can be easily located. Five main experimental thrusts are reported herein with references provided to more detailed publications. In the first, section 2 Plasma Scenarios, mostly related to the plasma core are reported with section 3 describing Fast Particle Physics. Moving outwards to one of TCV's strongest research roles, *scrape-off layer* and Edge Physics, section 4, and then specifically Divertor Physics, section 5 are treated. Section 6 describes advances and uses in Real-Time control that include feedback on RT-diagnosed plasma scenarios, AI-assisted discharge operation and disruption avoidance with section 7 providing a short introduction to some of TCV's near-future plans.

2. Plasma scenarios

TCV's shape control can match ITER Base-Line (IBL) strongly shaped configuration ($K \sim 1.8$ $\delta \sim 0.5$) as used on JET and AUG. ELMy discharges, limited using Ohmic heating alone, to $q_{95} < 3$ were extended with additional NBH for $q_{95} > 3.5$. Discharges often terminated violently following NTM activity triggered by edge localised mode (ELM) events [4]. By entering H-mode at lower Ip, and/or lower triangularity, generating smaller ELMs with reduced MHD activity, the accessible IBL discharges were extended with higher Greenwald fractions (f_g) obtained with N_2 seeding. Lowering the upper triangularity (0.45 –> 0.35) resulted in smaller ELMs with reduced ΔW, consequently reduced NTMs, but also a reduction in β_N. The addition of X3 heating clearly helped stabilise the NTMs with record reaching IBL triangularity ($\delta \sim 0.5$) with $H_{98} > 1$ and $f_g \sim 0.6$ The operational range was greatly expanded (e.g. for collisionality, $\nu^*(0.8)$: 0.23–5) together with X3 heating and N_2 seeding, although a high f_g, and consequent lower electron temperature (Te), made X3 coupling poor. A future development path will experiment

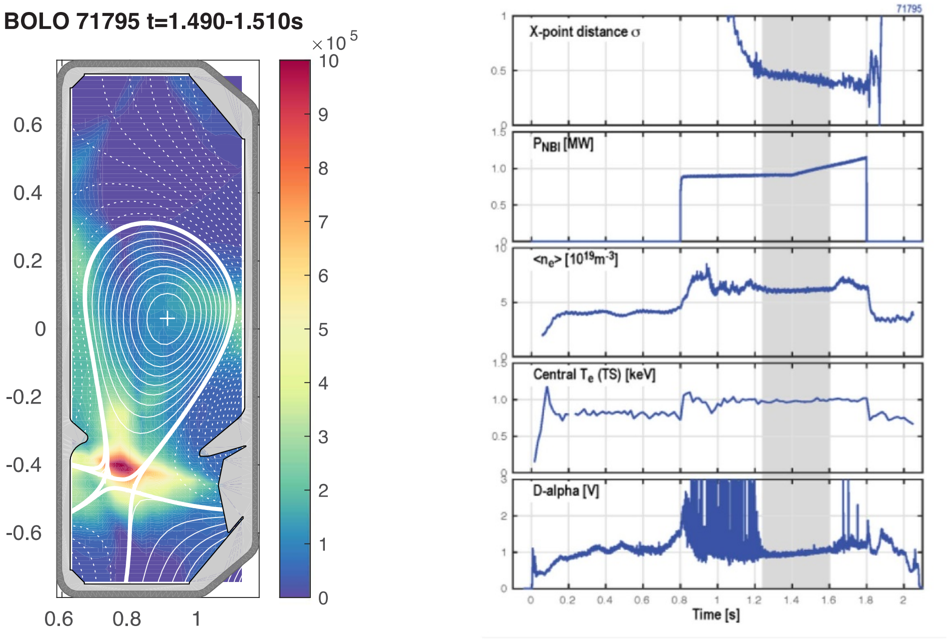

Figure 1. LHS: Bolometer inversion image of XPR radiator in an H-mode snowflake configuration. RHS: Plasma traces show ELM-free period is maintained from 1.2 to 1.6 s over a mild NBH power ramp.

with impurity gas quantity and efforts to couple more X3-powered NTM stabilisation.

Reducing the impact of ELMs remains vital to H-mode operations. X-point radiators, with an impurity seeded region in the vicinity of the X-point, have long been studied on TCV [5]. Although an X-point radiator (XPR) was not predicted possible in H-mode [6], such an H-mode XPR was found using N_2 seeding [7] albeit with a certain tendency towards a MARFE and/or an H $->$ L mode induced discharge termination. Some periods of full ELM mitigation were thus obtained over a limited operational range. Access to this regime was widened for an XPR in snowflake configurations (SF) and further still by placing the X-point beyond the throat of a baffled TCV divertor (see below), figure 1. This configuration was stable to changes in auxiliary heating and plasma shape and will be the subject of further investigation. The XPR did not affect the H-mode confinement, although some increase in Z_{eff} was observed.

H-mode, and thus ELMs, were avoided completely in negative triangularity (NT) discharges attaining record, albeit transient, $\beta_{\mathrm{N}} \sim 3$ [8]. NT configurations have been explored on TCV since 1993, as TCV can naturally operate over a wide ($-0.6 \leqslant \delta \leqslant 0.6$) range of triangularity. This is further enhanced by TCV's shaping control allowing separate variations of the upper and lower triangularities. Both HFS-limited and diverted NT configurations were explored with both NBH and ECH heating and discharges over a wide parameter range that included Ti $>$ Te [8, 9]. In TCV, NT discharges can achieve equal, or sometimes better than, H-mode performance unlike classic positive triangularity (PT) configurations, but appear more vertically unstable than PT, although it should be noted that TCV's vacuum chamber shape is not optimised for NT, figure 2. Although a pedestal formation is supressed, they can attain higher confinement and lower core transport than TCV IBLs with less heating and, of course, no ELMs. Edge turbulence with NT appears reduced, and an independent scan of upper and lower (X-point) δ indicated improving confinement primarily for upper negative δ. Low Z impurity and momentum transport showed steeper gradients when increasing NT in contrast to PT indicating a possible onset of TEM over ITG turbulent nature [10]. Vertical stability and density limits are described in another paper at this conference [9]. Obtaining a reliable detachment with NT is hampered by vertical stability issues, a tendency to exceed β limits and a narrower divertor target than for an equivalent PT configuration (see below).

Core confinement studies addressed for PT L-Mode. Linear and saturated ohmic confinement (LOC/SOC) confinement saturation, often seen correlated with intrinsic toroidal rotation reversals and a change in turbulence regime, was probed for D, H and He working gases [11]. Correlation of these phenomena, often only reported with D working gas, was not obtained with H and He bulk plasmas although clear LOC/SOC transitions were observed implying these phenomena do not have the same cause. This was further supported with NT/PT comparisons where, although, again, a LOC/SOC transition was always located, NT discharges did not display a rotation reversal where, here, such a reversal is more easily associated with a change in the rotation profile's slope than its absolute value [11].

H-mode confinement and pedestal studies were extended to low collisionality using strong ECH and long-pulse, high β_{N} discharges. High bootstrap avenues emulated on TCV for machines like JT60SA and DEMO progressed where, sustained using electron cyclotron current drive (ECCD), steady state electron iternal transport barrier with NBH and NBH driven H-mode configurations with off-axis co-ECCD were obtained. A transient $\beta_{\mathrm{N}} \sim$ 2H-mode was achieved with the

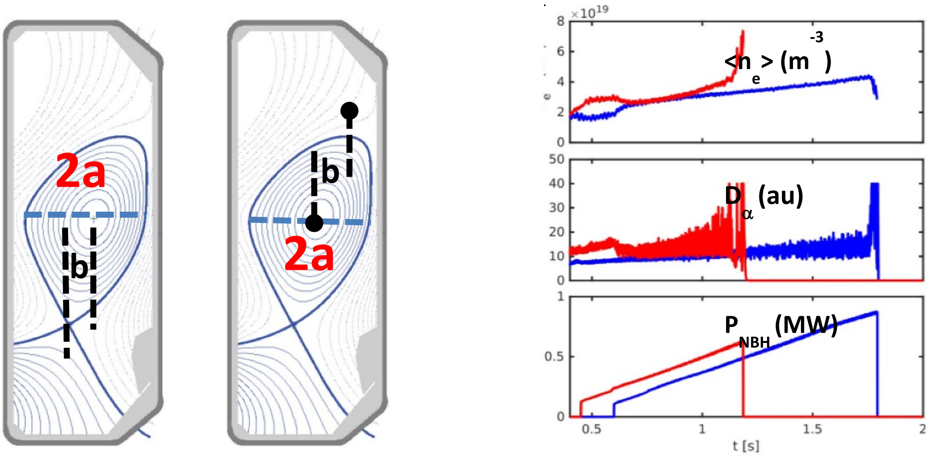

Figure 2. LHS: Cartoons showing lower and upper triangularity = b/a, RHS: NT (blue) does not go into H-mode like PT (red) during NBH ramp that far exceeds the threshold power for PT H-mode transition.

first stationary, fully non-inductive, ITB and NBH reaching $\beta_N \sim 1.8$ [12] suggesting further possible improvements may yet be found by merging these approaches, using the increased available ECH and NBH power, to operate with a double-confinement barrier.

A theory-based re-assessment of the 'Greenwald' density limit in Tokamaks [13], here based on turbulent transport, was performed [14]. A multimachine database of density limits showed that the increase of the boundary turbulent transport with the plasma collisionality sets the maximum density in tokamaks that would imply a strong dependence on heating power. This would predict a significantly higher safety margin on the attainable core density than the Greenwald empirical scaling in most reactor scenarios that are currently modelled to have to operate close to, or even above, that limit.

3. Fast particle physics

With a view to reactor operation, research into the physics of disruptions, runaway electrons (REs) and fast ions (FIs) was addressed. Dependable RE scenarios were found that featured near-full plasma current pre-disruption conversion, at disruption, to long duration RE beams characterised for impurity species massive gas injection (MGI) of (Ne, Ar, Kr) with a 200 kA RE beam was maintained for over 1 s [15, 16]. This beam was stable enough to undergo a position-controlled ramp down until ~20 kA when vertical stability control was finally lost. The central solenoid Ohmic drive was employed to maintain, examine the natural decay time of, and even ramp down the post-disruption RE current until the vertical-control limiting final disruption. A second, larger, MGI pulse during the RE beam phase, that is being considered as an option to mitigate the potentially dangerous RE beam, increased the RE ramp down rate, but only roughly proportionally to the increase in measured electron density rather than the injected gas quantity. RE beam formation was found harder after increasing the pre-MGI elongation and lower pre-MGI plasma currents and a seemingly hard limit of $K \leqslant 1.5$ for a RE beam, related to the stability and control of elongated plasmas, was identified. RE beam formation was dependent upon a sufficient pre-MGI RE seed, large enough to sufficiently increase the plasma conductivity created by operating at low plasma densities ($n_{e,0} < 1 \times 10^{19}$ m^{-3}) [16].

With a reliable recipe for RE beam formation, the problem of benign termination, to avoid post disruption damage in future machines, was addressed [17, 18]. By injecting deuterium gas, the RE-beam companion plasma recombines (the measured plasma density decreases drastically) until an MHD instability is triggered that then expels the beam over a large range of angles/inner vessel surfaces, avoiding the feared damage of a localised beam termination. This MHD instability was engendered using 'compression' with the RE beam displaced onto and then into the central column, (here, q_{edge} is the safety factor at the limiting central column), by increasing the RE current or by decreasing the toroidal magnetic field. A q_{edge} descending to near $q = 2$ was often required to obtain this MHD although a value of q_{edge} of 3 was also sometimes seen. The injected pressure was varied over a 0.05–1 Pa range but no inter-machine (JET, AUG and TCV) clear scaling for the optimal pressure was found although higher plasma densities were found to increase the wetted target areas, reducing the resultant target temperatures. A non-linear neutral pressure increase for recombination was found to depend upon RE current, impurity quantity and main plasma species. Excessive deuterium injection reversed this trend, figure 3, ascribed, to a decrease in the companion plasma temperature, and increased plasma resistivity, from increased collisions of the injected gas with the RE. The test for successful RE mitigation is taken during the final current quench where the stored kinetic and magnetic energy must be dissipated. Ideally, the RE beam dissipates by heating the companion plasma, reflected by longer quench times and a higher radiated power fraction. Over an order of magnitude reduction in the non-mitigated wall heat fluxes have already been reported that scale well with higher RE currents. Companion experiments have also shown that

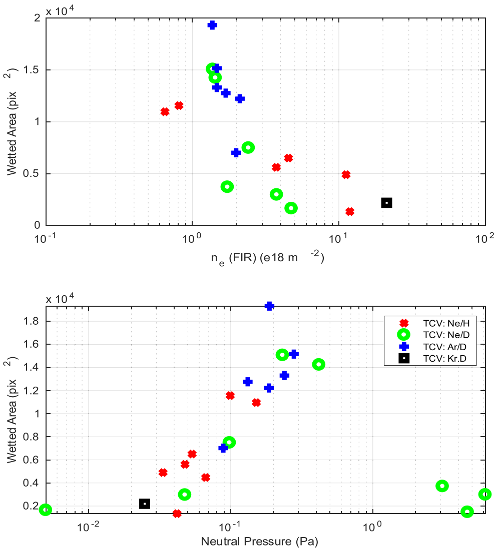

Figure 3. RE wetted area as function of core (upper figure) and neutral (lower figure) densities- note roll over in initial liner trend with increasing neutral pressure. Adapted from [17]. © The Author(s). Published by IOP Publishing Ltd. CC BY 4.0.

ECH during, or even following, RE beam formation can also strongly mitigate the RE beam, offering another possible path to RE beam mitigation [16].

Alfvén modes, stimulated by the 25 kV NBH, were qualified using changes in beam energy and/or toroidal magnetic field together with linear kinetic stability code calculations [19], with an estimation of the fast particle distribution function modelled using the TRANSP/NUBEAM code. The recently commissioned 55kV 1 MW tangential neutral beam also generated a rich Alfvénic spectral response on magnetic probes and on an upgraded FILD head, now equipped with a 128-channel imaging avalanche photodiode detector (APD) FILD-target imaging camera. Comparisons of neutron emission rate deficits, compared to ASTRA simulations, correlate with the Alfvén signal measured by a fast magnetic probe [20]. Centrally deposited X2 ECH (with or without an ECCD component) was able to stabilise this Alfvénic activity with a corresponding recovery of the measured neutron rate. The FILD detector only registered a signal when, with a clear Alfvén mode present from high power NBH heating, a low power (100 kW) 48kV radially injected diagnostic beam was also present, (essentially a 'probe' beam), particularly for high pitch angles. To date, NT configurations show considerably less toroidal Alfvén excitation activity, but it should be noted that, with tangential injection, the NBH deposition profile is radically altered. Toroidal field and upper triangularity in NT configurations scans showed changes in the FILD signal amplitudes varying nearly linearly with the edge measured magnetic perturbation amplitude, again preferentially affecting higher measured FI pitch angles. FILD signals, already reported to be modulated by sawteeth instabilities, NTM and most probably other MHD activity, is being modelled with ASCOT and the measured FILD entrance slit geometry in an attempt to model the orbit-origin of the strong features (clear stripes) observed on TCV FILD systems and in publications from other machines.

4. Sol and edge physics

Advances in SOL and edge physics over this period were, in particular, due to a diagnostic array augmented to monitor the, still relatively spatially open, divertor region within the TCV vessel. These can probe standard SND (e.g.: IBL) discharge shapes and the vast array of TCV's divertor configuration research targets. TCV's Langmuir probe array has been extended to cover most of the vessel's poloidal section and the new baffle surfaces were equipped with additional Langmuir probes and bulk-embedded thermocouples. Understanding the machine power balance has also progressed with a reworked, single poloidal position RADCAM multiple line-of-site camera array (AXUV, Soft-X and Bolometers) [21] and the divertor probed by a novel reciprocating Langmuir probe array (RDPA [22],) and a multi-tipped legacy reciprocating probe able to, briefly, cross the last closed flux surface (LCFS) [23]. Spectroscopy diagnostics for TCV's divertor have evolved drastically. The multi-spectral 2″ bore MANTIS 10-camera divertor system was augmented by 2× 6-channel MANTIS II 1″ bore compact optical versions [24]. Divertor spectroscopy (DSS) now includes high resolution multi-chord observation fans that can measure radiating-ion temperatures to well below 1 eV. Finally, tomographic inversions of the video images sped up over 100× using GPU software that can now, for instance, use all 3 MANTIS camera images of the same spectral feature to be tomographically inverted self-consistently, that greatly reduced the strength of inversion artefacts. In turn, work on mathematically improving these inversions, using external information, such as the poloidal field reconstructed geometry or other spectral information, promises to improve both the quality and reliability of these tools. This methodology will also propagate estimates of the likelihood of the deduced inversions to provide uncertainty estimates for deduced plasma parameters [25].

It is, however, in bringing these diagnostics together that the biggest advantage is seen. Experiments that scanned the divertor Thomson-scattering chords (able to measure Te < 1 eV) in small steps across the divertor leg [26–28] were compared with values of Te and Ne from MANTIS Balmer series intensities and Helium spectral line ratios taken from one spectral line, or, together. Uniting these interpretations, MANTIS images were validated against Thomson measurements with sufficient quality to both challenge existing collisional radiative and divertor modelling and identify validated plasma parameter ranges for this spectroscopic 2D-plasma parameter estimator, figure 4.

The main detachment physical processes were probed by performing these comparisons across the range of core density ramps associated with detachment research. This method can now be reliably applied to the wide range of TCV's divertor configurations even where Thomson measurement access

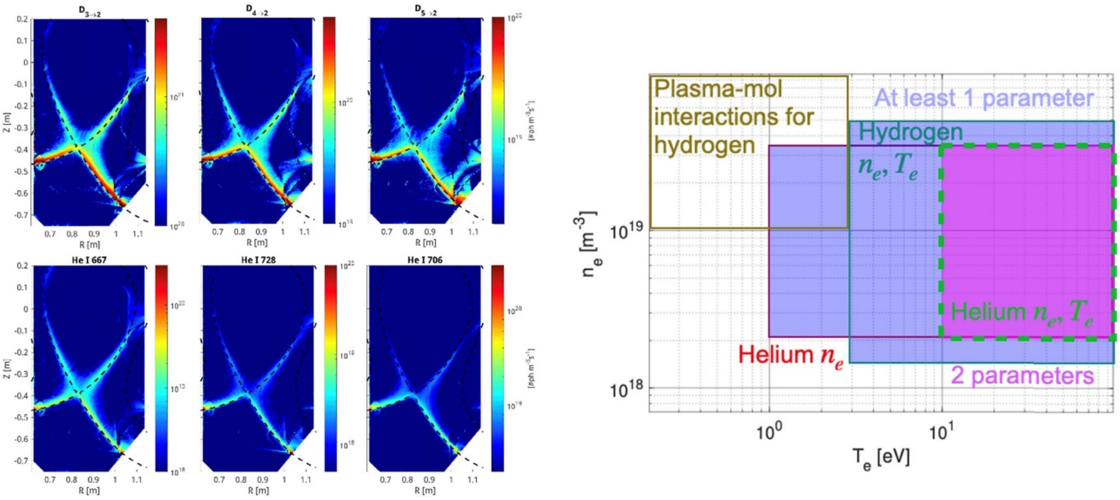

Figure 4. LHS: MANTIS inverted emissivities from 3 D spectral lines (top) and 3 He spectral lines (bottom) RHS: Thomson scattering validated regions where data can be combined to generate 2D Ne & Te plasma divertor maps. Where D and He data can both be used, the deduced parameter uncertainties decrease strongly.

is not available [29]. Line emission profiles across the divertor obtain spatial resolution along and across the divertor are used to interpret the line integrated spectroscopy of TCV's DSS, figure 5. Differences, and similarities, between a range of impurities' ion temperatures and electron temperatures with and without Thomson add a whole new dimension to model comparison, generating a more complete picture of the divertor state, including estimations of particle/impurity transport, of the divertor processes as the divertor evolves towards a detached state. Clear differences between present models and experiment are seen, in particular with respect to molecular recombination processes that can enhance plasma cooling at higher temperatures than volumetric recombination would allow. A Coherent Imaging System is being constructed to augment this picture with divertor flow measurements for a range of neutral and charged emitting species [30].

TCV's gas puff imaging (GPI) system that measures the light emitted from the edge plasma reaction to injected neutral deuterium or helium gas at TCV's midplane was augmented by a second system puffing orifice built into the tip of the divertor baffles [31, 32]. Using the outer midplane GPI system and a RDPA in the divertor region, the size, radial velocity and parallel extension of SOL filaments in TCV were measured [33–36] for discharges both in attached and detached conditions for a LSN L-mode configuration. Increasing core density generated filaments of increased size (∼60%) and radial velocity (∼100%) with no significant change in the filament detection frequency. Cross-correlation between the GPI and the RDPA was used to diagnose the parallel extension of filaments. Filaments in discharges with lower core densities in the near SOL did not extend into the divertor region, whereas filaments at higher densities always connected to the divertor region, figure 6. GPI systems were used to characterise the turbulent ejection of plasma at the midplane and towards the divertor region. By relating the measured filament brightness fluctuations as functions of the locally fluctuating electron temperature and density, the ejected feature strengths could be tracked from ejection at the midplane to regions beyond the LSN X-point. The GPI was mounted on MANTIS's lower divertor view and using TCV's position control to displace the LSN configuration across the GPI field of view allowed a full 2D picture to be built. This picture remains complex. At the midplane, a low fluctuation level radially just outside the LCFS is followed by a growing fluctuation level moving outwards. This trend, remarkably, is seen in regions above and below the X-point through to the divertor leg region although the ratio of intensity fluctuation standard deviation to mean intensity is higher above the X-point. Around the X-point, filaments that follow the field lines and others that move far to the LFS are observed. Furthermore, the small-scale turbulence seen in the divertor leg is not found to be correlated to structures above the X-point implying further cause-effect complexity.

Preliminary estimations indicate that these divertor 'blobs' can contribute considerably to the profile broadening at the divertor targets. Elongated filaments just above the X-point and in the far divertor SOL were observed whose shape and motion matched field line tracing from the outboard midplane. Their reduced occurrence in the divertor indicates that not all these far-SOL filaments reach deep into the divertor, and that these contribute only to the outermost part of the target profile.

5. Divertor physics

TCV continues to vigorously pursue outstanding issues in plasma exhaust physics. The central element of recent TCV upgrades, within the EUROfusion exhaust (PEX) mandate, is the installation of physical, carbon protection material, gas baffles inside the TCV vessel to impede the passage of neutrals between the region encompassing the core plasma from that containing the divertor's strike points [37, 38]. This was accompanied by the installation and/or upgrade of many state-of-the-art diagnostics to probe the exhaust from the core plasma to the strike points with the goal of mitigating the strike

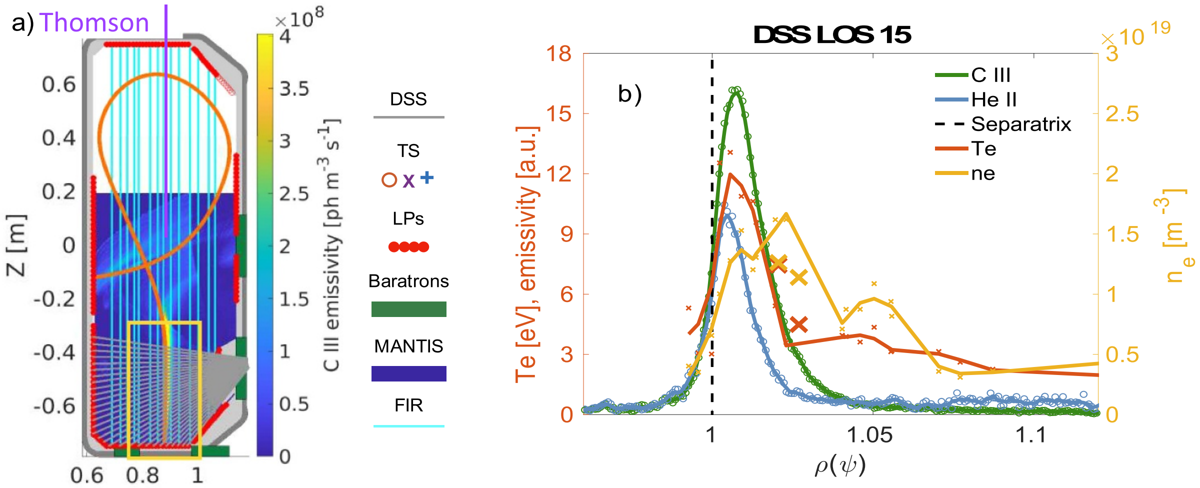

Figure 5. LHS: DSS spectroscopy chords matched to divertor position which is then scanned (using TCV's excellent plasma position control) across the Thomson laser path. Many diagnostics, together with MANTIS are used to quantify the reference plasma. RHS: Validation divertor scans and MANTIS inversion are combined for one DSS chord at one time to provide simultaneous spectral line emission and plasma parameter profiles. In the validation experiments these profiles were tracked as the plasma conditions approached detachment.

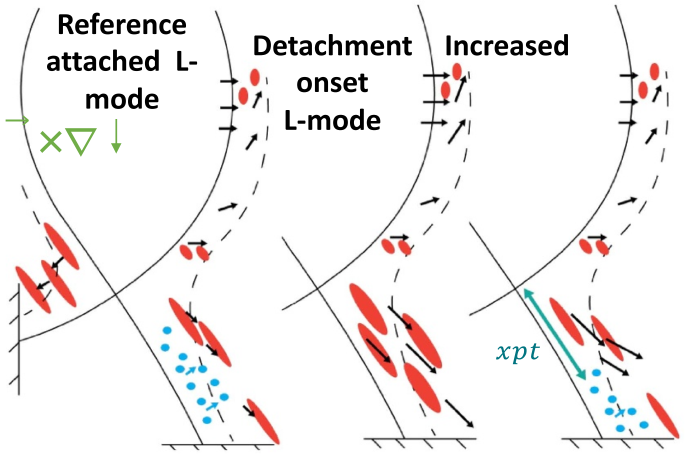

Figure 6. Divertor near-SOL generally feature divertor localized filaments. Divertor localised filaments (blue dots) disappear during detachment. Reproduced with permission from [32].

point power density to tolerable physical levels [37–39]. The initial baffle dimension choice, guided by SOLPS modelling, was augmented by new, longer and shorter, inner and outer baffles. Combinations of these results, including a legacy 'no-baffle' configuration, were compared to models with particular emphasis on their ability to establish a high neutral compression between the core and divertor regions with the simultaneous goal of remaining compatible with a high-performance core plasma, yet radiatively dissipating an increasing, considerable, fraction of the exhaust power from the X-point, across the divertor region(s), up to the strike points, termed detachment.

Due to the extraordinary wealth of information generated during these experiments, only some main results of divertor baffling can be reported here [37]. Increasing the divertor closure, together with placing the X-point such as to best benefit neutral divertor compression, successfully led to a cooler divertor with a reduction in target power fluxes. Using repeat plasma exhaust (PEX) discharges in all baffle configurations, neutral pressure gauges reported an, up to, 5× increase of the divertor neutral pressure (for the longest inner and outer baffles) and reduced fuelling through the divertor to the core plasma, that facilitated access to detachment at lower core plasma densities. These experiments employed a programmed core density ramp, often until the discharge density limit, to parameterise any changes in the divertor. Figure 7 shows the divertor density measured by a floor positioned Baratron for unbaffled, short inner/outer and longer inner/outer baffles as a function of a core density ramp of the working D gas. Reducing gas conductivity from the divertor resulted a lower core density peaking for the L-mode discharges. Increased divertor baffling lead to higher divertor pressures that, in turn, decreased the core density required for divertor detachment monitored by floor IR images and the position of the CIII radiation front [39]. Studies were extended to H-mode configurations and the addition of radiating impurity gasses (N, Ne) into

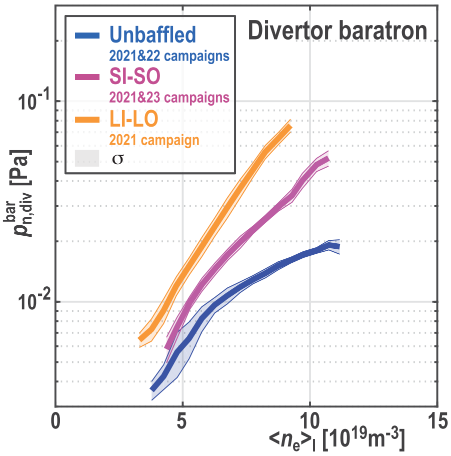

Figure 7. Divertor pressure from floor mounted baratron as a function of core density during a pressure ramp. Traces for unbaffled, short inner/outer (SI–SO) and longer inner/outer (LI–LO) baffles are shown together with uncertainties shaded in grey (σ). Increased divertor pressure corresponds to earlier divertor detachment [37].

the divertor region to further enhance divertor cooling where, even with only a shorter inner baffle, a 40% decrease in power to the strike points was obtained. These ongoing experiments also benefitted from four additional poloidally, and three toroidally, distributed gas valves to probe differences between working gas and/or impurity injection into the main, divertor common and divertor private zones.

Divertor studies examined how alternative divertor configurations mitigate target power, facilitate detachment together with a wider detachment operational window and increase the radiated power whilst retaining a high-performance plasma core compatibility. Two main configuration approaches were studied: geometries to optimise X-point radiator access and operation and long-legged divertors that seek to generate a strongly radiating zone between the divertor target and the X-point. The former will have cost issues relating to the more complex magnetic configuration and the latter may not make the best use of the costly main toroidal field volume. SF configurations, with two nearby X-points, found up to a 2/3 reduction in the target heat loads [40]. Strangely, this improvement was strongly reduced with N_2 seeding and no advantage in the core for the SF, over a SND configuration, was obtained with increased N_2 seeding, even though the SF's radiating zone was farther from the LCFS. Initial EMC3-EIRENE modelling had indicated a higher required cross-field transport to match experiment [38]. A 20% reduction in target power for a baffled over unbaffled SF, with a little more divertor radiation, was countered by an increased N core pollution that, however, diminished with decreasing inter X-point separation. Access to a stable XPR regime was, however, facilitated with a SF configuration, that was ascribed to the higher flux expansion around the X-point. Some of these plasma shapes, also accessed a completely ELM-free operation, even across a power ramp, figure 1.

Other observations that were noteworthy in this research are reported for completeness. Using the MANTIS CIII front position as a detachment proxy, a smaller than predicted reduction in the detachment threshold [33, 41] was found, from increasing flux expansion alone, that was partially explained by including parallel flows [42].

Small (SN) and high (XD) flux expansion H-modes were compared with an X-point divertor (XPT). Here, the H-mode core performance ($H_{98} \sim 1$) was similar in all cases with a 50% decrease in the inter-ELM flux for the XPT observed, albeit with a strong dependence on the XPT's X-point separation. Together, Baffles, XPT and N2 assisted detachment resulted in over 95% decrease in the inter-ELM peak heat flux when compared to an attached SN case [43]. Finally reported in this shortened list, a study of detachment in conventional SN discharges was extended to include double-null (DN) configurations [44] where a 30% improvement was found in the peak heat load and a substantial reduction (20%–25%) in the detachment threshold together with a 50% higher radiation fraction. This came with a modest (10%–20%) reduction in the density limit. Even the modest effect of increasing poloidal flux expansion on detachment for the SN configurations was absent for the DN configurations.

Two further studies are briefly described. Detailed 2D Langmuir probe measurements, using the RDPA, over a large part of the TCV divertor region measured plasma density, temperature, potential and parallel Mach number distributions [22, 45]. Estimations of vertical particle flux densities associated both with parallel flows and $E \times B$ flows were used to assess the divertor particle balance for Ohmic L-mode plasmas in both baffled and non-baffled divertor configurations. A range of divertor regimes were accessed by varying the plasma line-averaged density. The study reveals that $E \times B$ drift contributions to the poloidal ion flux can be comparable, and sometimes larger, than the ion flux along the magnetic field lines. A detailed divertor particle balance, with and without baffles, indicated that the outer target flux originates from ionisation along the divertor leg. In the second, a comparison of self-consistent full-size turbulent-transport simulations of the divertor and SOL was undertaken on the so-called TCV-X21 series of L-mode discharges that featured both toroidal magnetic field directions and data from TCV's diagnostic array including the RDPA [22] and the fast-reciprocating probe [46]. The discharges were operated at lower-than-normal toroidal field (0.95 T) to decrease modelling computational cost and at low density, in sheath-limited conditions. Simulations were performed on the same data set with the GBS, GRILLIX and TOKAM3X 3D two-fluid drift-reduced Braginskii turbulence codes [47], references within] and validated whilst considering each diagnostic's uncertainty together with each simulation's uncertainty [48]. A table of code and simulation results was analysed with significant matches to experiment encouragingly found at the outer midplane. It is to be noted, however, that simulation results were often outside experimental uncertainties at the targets and across the divertor volume. Although many qualitative tendencies were reproduced, many compromises in boundary conditions and scale lengths were chosen to run the simulations. It is expected that additional physics will be required before these models obtain quantitative matches to the TCV-X21 data set.

6. Real-time control

TCV's real-time control system structure has been reworked within the MARTE2 framework using a reflective-memory backbone [49]. The addition within this real-time framework of complex diagnostics, such as Thomson Scattering and Video (MANTIS) information was complemented by an EtherCat field bus extensions that control the ECH mirror orientations, NBH injection energy/power and the full tokamak magnetic coil control set. Controllers are built in a modular fashion under Matlab/Simulink using a new open-source framework that are now strongly parameterised such that coefficient changes no longer require controller recompilation. This abstraction has encouraged external scientists to develop algorithms offline then install/exploit/compare them directly on TCV with little additional on-site adaptation required. Basic modules include RT-LIUQE [50] sub-millisecond fast magnetic reconstruction, the RAPTOR and RAPDENS plasma simulator together with diagnostic observers that run routinely upon which other controllers can rely. Three strong, but overlapping, usages for this system are reported. TCV's legacy plasma control is based upon a fixed boundary calculation of coil current references and observers in multiple PID feedback loops. RT-LIUQE has previously been reported as an improved observer of the actual shape and plasma position and a rigid, linearised, plasma response model for the TCV tokamak has successfully guided the machine control parameters to improve shape and position control fidelity [51]. This was extended to SF configurations, where the X-point separation control is paramount to improve the SF configuration stability [52]. In view of TCV's high vessel aspect ratio and frequently requested access to highly shaped plasma configurations, vertical plasma control, particularly for higher elongation, has always been one of TCV's challenges [53]. Fast coils, inside the TCV vessel, are used in combination with the external poloidal coil set to stabilise the higher growth rates associated with high elongation. The legacy control approaches, that only used subsets of the full poloidal coil set for vertical control, were improved to include all coils after a control-theory analysis of high frequency vertical position excursions with an optimised coil combination employed for derivative control and a different coil combination for proportional control [54]. The resulting controller both improved the vertical control and reduced the work required from the poloidal coil array. For the future, better general vertical controllers will be designed together with controllers optimised for specific needs that will include plasma shape and position together with the dynamics resulting from auxiliary heating systems and their own dynamics.

Control of the CIII radiation front in TCV through deuterium and/or nitrogen divertor gas injection was developed for TCV's detachment experiments [56]. This work modelled the reaction of the plasma CIII front position, deduced from the MANTIS cameras, to the gas valve actuator(s) to generate, offline, a reliable and efficient controller, then implemented on TCV. The technique was extended to NII-radiation front control whose position varies similarly to CIII but is situated closer to the divertor target representative of a colder plasma [57]. Here nitrogen was used as the only injection gas or only as a trace gas for comparison with deuterium injection to control the NII front position to track a requested temporal evolution of the NII front position and the plasma core density. With NII it was possible to track deeper into detachment where the CIII front had already reached the X-point and contrast the effect of the more strongly radiating N_2 injection from deuterium injection on the power to the inner and outer strike points. These system identification techniques were applied to a multiple in, multiple out (MIMO) control problem where the plasma core density and NII radiation front condition, (the new detachment proxy), were controlled together by separate N_2 and deuterium gas injection actuators that affected both sought parameters [55]. Linear combinations of deuterium and N_2 injection were found, from system identification of each injection's response, to linearise the controller response in the range of interest such that these 'virtual' actuators were now, effectively, decoupled. In the resulting TCV experimental demonstration, the MIMO injection was provided by a combination of two PI controllers on the virtual actuators that controlled both the NII front position and core plasma density through a strong density ramp, figure 8. This is the kind of separate divertor and core plasma control that will be necessary to operate fusion reactors. Using the same digital control approach, direct plasma control on RT-LIUQE magnetic reconstructions was used to effect in NT discharges where NBH injection, that also fuels the plasma efficiently, increases the plasma β towards NTM triggered disruptions [8]. With feedback on the NBH power, long periods of controlled, and high, β were explored whilst compensating for the direct fuelling changes engendered from the evolving NBH power.

Machine learning has been applied to TCV research in several ways. Disruption avoidance, necessary in any reactor grade machine, is complex and relies upon estimating, through combinations of observable and RT-modelled parameters, a 'proximity' to disruption. A combination of machine-learning (ML)-based and physics-based algorithms has been developed to estimate the proximity of the plasma discharge to events in real-time [58]. Control algorithms, such as changes in the power and/or orientation of auxiliary heating, plasma density or position and shape control are triggered depending upon the plasma state by a supervisory control framework. Often the very regions where disruptions are more likely are those that research wishes to attain, making the plasma discharge trajectory choice even harder. Off-normal (unpredicted) events are not uncommon and, finally, choosing the optimal mitigation scenario for each disruption occurrence is the only solution [59]. With a limited number of actuators available, a supervisory framework [60] was developed with a customisable decision logic that can switch between different control scenarios, with multiple choices of actuator usage, depending upon the nature of the situation. In the same vein, after demonstrating NTM stabilisation by precise X2 ECH and ECCD deposition near rational q surfaces [4], robust application to a range of possibly moving plasma configurations, with insufficiently reliable RT magnetic reconstruction, was addressed. A simple solution, with a small sinusoidal radial sweep of the EC power, alleviated some of the high beam alignment requirements [61].

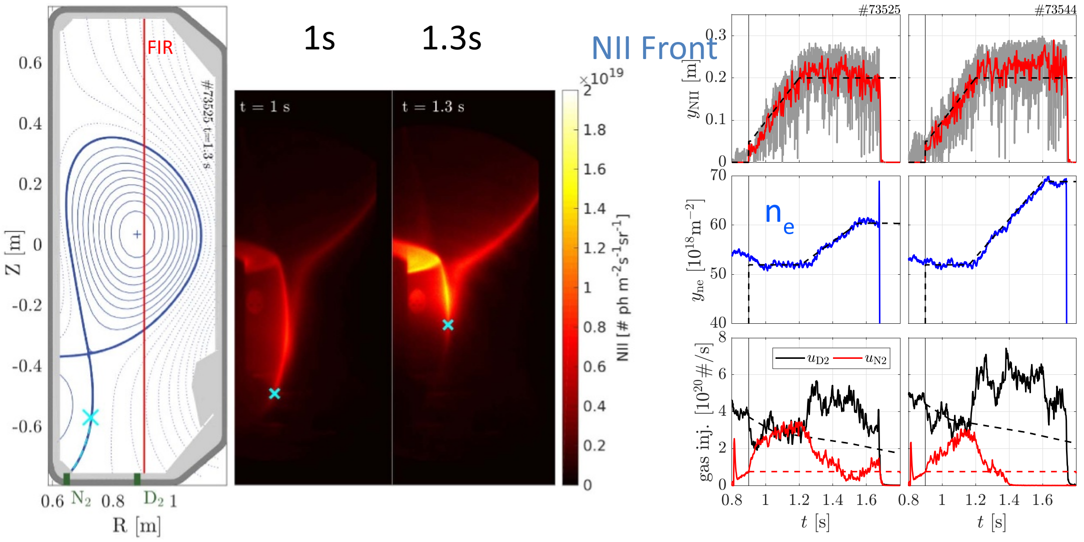

Figure 8. LHS: Plasma density and NII radiation front position tracked in RT by FIR and MANTIS diagnostics RHS: two examples of Ne (top) & NII position tracked (dashed refs) with virtual gas actuator traces that are linear combinations of the D and N injection chosen to orthogonalise the plasma reaction. Adapted from [55]. © 2023 The Author(s). Published by IOP Publishing Ltd on behalf of the IAEA. CC BY 4.0.

A new NTM prevention strategy, that only required transient EC power near the relevant rational surface, proved effective for preventing ST-seeded NTMs. A study of the physics of this stabilisation indicated that its success resulted from local effects of the EC beams rather than global current profile changes. Clearly, combinations of engineering-like solutions to render physics-based plasma control sufficiently robust for reactor operations will require further work.

In another direction, deep reinforcement learning was applied to generate a magnetic controller based only on trial-and-error interaction with a free-boundary tokamak simulator [49, 62]. A plasma discharge designer first specifies experimental, with the possible inclusion of time-varying, control goals. The deep reinforced-learning (RL) algorithm then uses the simulator to locate an efficient policy to meet these goals. Finally, this control policy, cast as a running neural network, is constructed that runs in real-time on relatively modest hardware through the available observers. A diverse set of plasma configurations was thus generated and operated on TCV, including elongated and conventional shapes, as well as advanced configurations such as NT, SF and even droplet configurations. The neutral network, in effect, replaced TCV's legacy 'multiple-PID' control systems to provide direct magnetic coil signals to the machine, figure 9. Experimental tracking of the location, plasma current and shape was demonstrated for these configurations indicating that, at the least, the Tokamak simulator had captured the necessary plasma dynamics and TCV machine specificities. For the ML community, this represents one of the most challenging real-world systems addressed by reinforcement learning and, since this technique employs no experimentally obtained data, it also demonstrates a path for initiating new experimental devices such as ITER and reactors such as DEMO.

This DeepMind approach has also been used to extend TCV's multiple X-point research to help identify an operating regime that extends the two nearby X-points of the so named 'snow-flake' configurations to three nearby X-points named a 'Jellyfish' [63], figure 10. Following initial attempts to identify an operational space within TCV for this, the novel deep RL architecture located such an initial space from where that configuration was further refined using this together with TCV's legacy control development strategies. This configuration is a new addition to TCV's research in changing connection lengths, flux expansion and power spreading further testing the limits of current divertor models.

7. Outlook

For 2024 and beyond, TCV will address new and legacy issues. TCV has been fitted with robust neutron and gamma-radiation shielding removing all restrictions on auxiliary NBH usage. Further auxiliary heating (an additional dual frequency (84/126 GHZ) Gyrotron, top/lateral launch) is under consideration; NBH, injecting over 4 MJ within a discharge, will advance NT scenarios, QCE and other reduced ELM regimes including zero applied torque or zero plasma rotation using spectroscopic Doppler feedback upon the opposed tangential neutral-beam geometry. All the subjects described herein will benefit from these augmentations in particular when managed by TCV's increasingly complete and wide seeing control system. Divertor modelling has indicated that further increasing the baffling of long-legged divertors would generate a much cooler target plasma than for present baffles, with a potential 3× increase in the tolerable exhaust power, figure 11 [37, 39, 64].

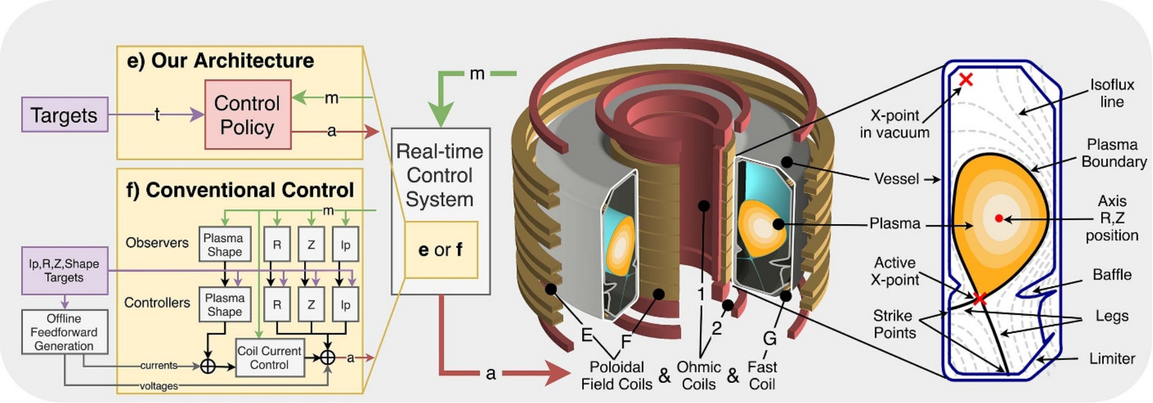

Figure 9. Schematic of the alternative paths running the TCV plasma control. Here the conventional control system that uses multiple observers and control algorithms (crossed out in red), is replaced by a control policy learned from a free-boundary tokamak simulator for a diverse set of plasma configurations. Adapted from [62]. CC BY 4.0.

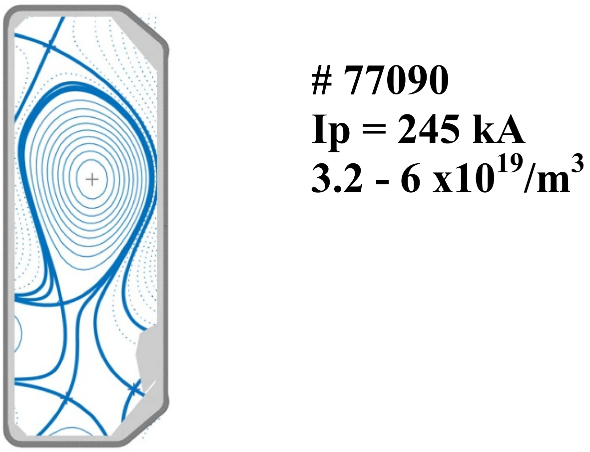

Figure 10. Example of a Jellyfish poloidal configuration with three X-points in the lower divertor region. LFS parallel connection length peaks ∼120 m. A strong reduction in peak heat flux compared to the reference single-null reference configuration. Adapted from [63]. CC BY 4.0.

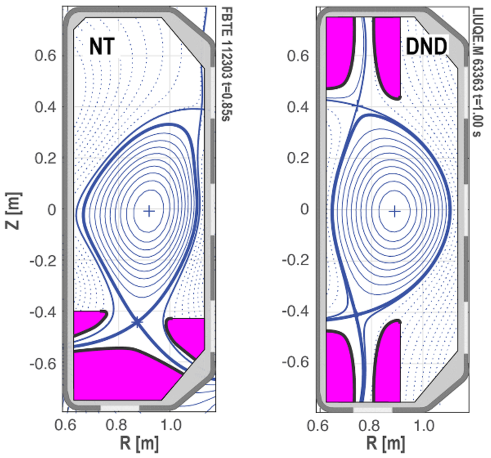

Figure 11. Example test poloidal plasma shapes (SN and DN examples shown) under consideration to increase neutral compression to increase access to deeply detached, high-power, configurations.

Such a tight baffle could be installed by replacing current internal protection tiles, similarly to the technique used in the present baffle experiments, with a further option installing upper and lower tight baffling to equip a DN, highly baffled, configuration. By nature, these solutions will be less accessible to current diagnostic arrangements, for instance radiation front detachment control using MANTIS, probably necessitating more in-vessel diagnostic installations. Successful compatibility of these high power divertor exhaust compatible solutions will depend upon maintaining high core performance that will target both PT, H-mode or NT, L-mode, configurations.

Acknowledgment

This work has been carried out within the framework of the EUROfusion Consortium, partially funded by the European Union via the Euratom Research and Training Programme (Grant Agreement No. 101052200—EUROfusion). The Swiss contribution to this work has been funded by the Swiss State Secretariat for Education, Research and Innovation (SERI). Views and opinions expressed are however those of the author(s) only and do not necessarily reflect those of the European Union, the European Commission or SERI. Neither the European Union nor the European Commission nor SERI can be held responsible for them. This work was supported in part by the Swiss National Science Foundation and in part by the US Department of Energy under Award Number DE-SC0010529.

ORCID iDs

B.P. Duval https://orcid.org/0000-0001-7783-129X
S. Coda https://orcid.org/0000-0002-8010-4971
J. Decker https://orcid.org/0000-0003-0220-2653
A. Fasoli https://orcid.org/0000-0003-4319-5736
O. Février https://orcid.org/0000-0002-9290-7413
T. Goodman https://orcid.org/0000-0002-2464-6303

B. Labit https://orcid.org/0000-0002-0751-8182
A. Merle https://orcid.org/0000-0003-1831-5644
P.A. Molina Cabrera https://orcid.org/0000-0001-6884-5833
A. Perek https://orcid.org/0000-0002-4117-0298
H. Reimerdes https://orcid.org/0000-0002-9726-1519
O. Sauter https://orcid.org/0000-0002-0099-6675
U.A. Sheikh https://orcid.org/0000-0001-6207-2489
C. Theiler https://orcid.org/0000-0003-3926-1374

References

[1] Hofmann F. *et al* 1994 Creation and control of variably shaped plasmas in TCV *Plasma Phys. Control. Fusion* **36** B277
[2] Fasoli A. *et al* (the TCV Team) 2019 TCV heating and divertor upgrades *Nucl. Fusion* **60** 016019
[3] Weisen H. *et al* (TCV Team) 2023 TCV tokamak neutron shielding upgrade for dual NBI operation *Fusion Sci. Technol.* **80** 1–13
[4] Felici F., Goodman T.P., Sauter O., Canal G., Coda S., Duval B.P. and Rossel J.X. (the TCV Team) 2012 Integrated real-time control of MHD instabilities using multi-beam ECRH/ECCD systems on TCV *Nucl. Fusion* **52** 074001
[5] Pitts R.A., Refke A., Duval B.P., Furno I., Joye B., Lister J.B., Martin Y., Moret J.-M., Rommers J. and Weisen H. 1999 Experimental investigation of the effects of neon injection in TCV *J. Nucl. Mater.* **266–269** 648–53
[6] Stroth U., Bernert M., Brida D., Cavedon M., Dux R., Huett E., Lunt T., Pan O. and Wischmeier M. (the ASDEX Upgrade Team) 2022 Model for access and stability of the X-point radiator and the threshold for marfes in tokamak plasmas *Nucl. Fusion* **62** 076008
[7] Bernert M. *et al* 2023 The X-point radiating regime at ASDEX upgrade and TCV *Nucl. Mater. Energy* **34** 101376
[8] Coda S. *et al* (the TCV Team) 2021 Enhanced confinement in diverted negative-triangularity L-mode plasmas in TCV *Plasma Phys. Control. Fusion* **64** 014004
[9] Sauter O. 2023 Negative triangularity tokamak operation in TCV *Preprint: 2023 IAEA Fusion Energy Conf.* (*London, United Kingdom, 16–21 October 2023*) [EX 1–3]
[10] Bagnato F., Duval B.P., Krutkin O. and Iantchenko A. (the TCV Team) 2023 Study of correlations between LOC/SOC transition, intrinsic toroidal rotation reversal and TEM/ITG bifurcation with different working gases in TCV *Nucl. Fusion* **63** 056006
[11] Bagnato F. *et al* (TCV) 2024 Study of impurity C transport and plasma rotation in negative triangularity on the TCV tokamak *Plasma Phys. Control. Fusion* **66** 075019
[12] Coda S. 2023 Developments towards high-beta, long-pulse scenarios in TCV and MAST-U *Preprint: 2023 IAEA Fusion Energy Conf.* (*London, United Kingdom, 16–21 October 2023*) [EX/P3-3]
[13] Greenwald M., Terry J.L., Wolfe S.M., Ejima S., Bell M.G., Kaye S.M. and Neilson G.H. 1988 A new look at density limits in tokamaks *Nucl. Fusion* **28** 2199
[14] Giacomin M., Pau A., Ricci P., Sauter O. and Eich T. (the ASDEX Upgrade team, JET Contributors, the TCV team) 2022 First-principles density limit scaling in tokamaks based on edge turbulent transport and implications for ITER *Phys. Rev. Lett.* **128** 185003
[15] Decker J. 2023 Recent progress in runaway electron research at TCV *Preprint: 2023 IAEA Fusion Energy Conf.* (*London, United Kingdom, 16–21 October 2023*) [EX/P4-3]
[16] Decker J. *et al* (the TCV Team and the EUROfusion MST1 Team) 2022 Full conversion from ohmic to runaway electron driven current via massive gas injection in the TCV tokamak *Nucl. Fusion* **62** 076038
[17] Sheikh U. 2023 Benign termination of runaway electron beams in the EUROfusion tokamak exploitation work program *Preprint: 2023 IAEA Fusion Energy Conf.* (*London, United Kingdom, 16–21 October 2023*) [EX/P3-5]
[18] Sheikh U. *et al* (ASDEX Upgrade Team and the TCV Team) Benign termination of runaway electron beams on ASDEX upgrade and TCV *Plasma Phys. Control. Fusion* **66** 035003
[19] Vallar M., Dreval M., Garcia-Munoz M., Sharapov S., Poley J., Karpushov A.N., Lauber P., Mazzi S. and Porte L. (the TCV Team) 2023 Excitation of toroidal Alfvén eigenmodes with counter-current NBI in the TCV tokamak *Nucl. Fusion* **63** 046003
[20] Karpushov A.N. *et al* (TCV Team) 2023 Fast-ion dynamics and instabilities on the TCV tokamak *EPS PPD* SPC/EPFL *49th EPS Conf. on Control Fusion and Plasma Physics* P5.093 2023 (available at: https://lac913.epfl.ch/epsppd3/2023/html/Fr/Fr_MCF93_Karpushov.pdf)
[21] Sheikh U.A., Simons L., Duval B.P., Février O., Moret D., Allegrucci A., Bernert M., Crisinel F., Tersztyánszky T. and Villinger O. 2022 RADCAM—a radiation camera system combining foil bolometers, AXUV diodes, and filtered soft x-ray diodes *Rev. Sci. Instrum.* **93** 113513
[22] De Oliveira H., Theiler C. and Elaian H. 2021 A fast-reciprocating probe array for two-dimensional measurements in the divertor region of the tokamak à configuration variable *Rev. Sci. Instrum.* **92** 043547
[23] Tsui C.K. *et al* 2022 Evidence on the effects of main-chamber neutrals on density shoulder broadening *Phys. Plasmas* **29** 062507
[24] Perek A. *et al* (TCV Team and Eurofusion Team) 2019 MANTIS: a real-time quantitative multispectral imaging system for fusion plasmas *Rev. Sci. Instrum.* **90** 123514
[25] Hamm D., Theiler C., Duval B.P. and Simeon M. 2023 Reaction-diffusion PDE-based framework for tomographic inversion of tokamak data *Swiss Physical Society*
[26] Martinelli L. *et al* (TCV Team) 2022 Implementation of high-resolution spectroscopy for ion (and electron) temperature measurements of the divertor plasma in the tokamak à configuration variable *Rev. Sci. Instrum.* **93** 123505
[27] Perek A. *et al* (the EUROfusion MST1 Team and the TCV Team) 2022 A spectroscopic inference and SOLPS-ITER comparison of flux-resolved edge plasma parameters in detachment experiments on TCV *Nucl. Fusion* **62** 096012
[28] Linehan B.L. *et al* (the TCV Team) 2023 Validation of 2D and measurements made with Helium imaging spectroscopy in the volume of the TCV divertor *Nucl. Fusion* **63** 036021
[29] Theiler C. 2023 Effect of magnetic divertor geometry on plasma exhaust and core compatibility in TCV *Preprint: 2023 IAEA Fusion Energy Conf.* (*London, United Kingdom, 16–21 October 2023*) [EX/P6-11]
[30] Bouwmans S. 2021 Camera based coherence imaging spectroscopy diagnostic for MANTIS to measure ion dynamics in TCV during divertor detachment *TU/e MSc Thesis* DIFFER (available at: https://pure.tue.nl/ws/portalfiles/portal/188046903/0892672_Bouwmans_S._MSc_thesis_MAP_MNF.pdf)
[31] Wüthrich C. *et al* (the TCV Team) 2022 X-point and divertor filament dynamics from gas puff imaging on TCV *Nucl. Fusion* **62** 106022
[32] Wüthrich C. *et al* 2024 Dependence of divertor turbulence on plasma density and current in TCV *Nucl. Fusion* Submitted
[33] Han W., Offeddu N., Golfinopoulos T., Theiler C., Terry J.L., Wüthrich C., Galassi D., Colandrea C. and Marmar E.S. (the TCV Team) 2023 Estimating cross-field particle

transport at the outer midplane of TCV by tracking filaments with machine learning *Nucl. Fusion* **63** 076025

[34] Offeddu N. *et al* (the TCV Team) 2022 Cross-field and parallel dynamics of SOL filaments in TCV *Nucl. Fusion* **62** 096014

[35] Offeddu N., Wüthrich C., Han W., Theiler C., Golfinopoulos T., Terry J.L., Marmar E., Ravetta A. and Van Parys G. 2023 Analysis techniques for blob properties from gas puff imaging data *Rev. Sci. Instrum.* **94** 033512

[36] Han W., Pietersen R.A., Villamor-Lora R., Beveridge M., Offeddu N., Golfinopoulos T., Theiler C., Terry J.L., Marmar E.S. and Drori I. 2022 Tracking blobs in the turbulent edge plasma of a tokamak fusion device *Sci. Rep.* **12** 18142

[37] Reimerdes H. 2023 Variable gas-baffling in the TCV divertor *Preprint: 2023 IAEA Fusion Energy Conf.* (*London, United Kingdom, 16–21 October 2023*) [EX/P2-17]

[38] Reimerdes H. *et al* (TCV Team and Eurofusion Team) 2021 Initial TCV operation with a baffled divertor *Nucl. Fusion* **61** 024002

[39] Reimerdes H. 2023 Results and implications of the TCV plasma exhaust (PEX) upgrade *EPS PPD* (available at: https://eps2023.github.io/EPS-2023-program.html)

[40] Gorno S. *et al* (TCV Team and Eurofusion Team) 2023 Power exhaust and core-divertor compatibility of the baffled snowflake divertor in TCV *Plasma Phys. Control. Fusion* **65** 035004

[41] Meineri C., Muscente P., Theiler C. and Galassi D. 2023 Numerical study of fully baffled Super-X L-mode discharges on TCV *Nucl. Mater. Energy* **34** 101383

[42] Carpita M. *et al* (the TCV Team) 2024 Parallel flows as a key component to interpret Super-X divertor experiments *Nucl. Fusion* **64** 046019

[43] Raj S., Bisai N., Shankar V. and Sen A. 2020 Effects of nitrogen seeding in a tokamak plasma *Phys. Plasmas* **27** 122302

[44] Février O. *et al* (the TCV Team) 2021 Detachment in conventional and advanced double-null plasmas in TCV *Nucl. Fusion* **61** 116064

[45] Oliveira H.D., Theiler C., Février O., Reimerdes H., Duval B.P., Tsui C.K., Gorno S., Oliveira D.S. and Perek A. (the TCV Team) 2022 New insights on divertor parallel flows, E × B drifts, and fluctuations from in situ, two-dimensional probe measurement in the tokamak à configuration variable *Nucl. Fusion* **62** 096028

[46] Tsui C.K., Boedo J.A., Février O., Reimerdes H., Colandrea C. and Gorno S. (The TCV Team) 2022 Relevance of E × B drifts for particle and heat transport in divertors *Plasma Phys. Control. Fusion* **64** 065008

[47] Oliveira D.S. *et al* (the TCV Team) 2022 Validation of edge turbulence codes against the TCV-X21 diverted L-mode reference case *Nucl. Fusion* **62** 096001

[48] Ricci P., Riva F., Theiler C., Fasoli A., Furno I., Halpern F.D. and Loizu J. 2015 Approaching the investigation of plasma turbulence through a rigorous verification and validation procedure: a practical example *Phys. Plasmas* **22** 055704

[49] Felici F. 2023 Advances in real-time tokamak control research on TCV *Preprint: 2023 IAEA Fusion Energy Conf.* (*London, United Kingdom, 16–21 October 2023*) [EX/P8-27]

[50] Moret J.-M., Duval B.P., Le H.B., Coda S., Felici F. and Reimerdes H. 2015 Tokamak equilibrium reconstruction code LIUQE and its real time implementation *Fusion Eng. Des.* **91** 1–15

[51] Anand H., Coda S., Felici F., Galperti C. and Moret J.-M. 2017 A novel plasma position and shape controller for advanced configuration development on the TCV tokamak *Nucl. Fusion* **57** 126026

[52] Anand H., Coda S., Felici F., Galperti C., Moret J.-M., Labit B., Reimerdes H. and Maurizio R. (the TCV Team) 2019 Real time magnetic control of the snowflake plasma configuration in the TCV tokamak *Nucl. Fusion* **59** 126032

[53] Hofmann F. *et al* 2002 Extension of the TCV operating space towards higher elongation and higher normalized current *Nucl. Fusion* **42** 743

[54] Pesamosca F., Felici F., Coda S. and Galperti C. 2022 Improved plasma vertical position control on TCV using model-based optimized controller synthesis *Fusion Sci. Technol.* **78** 427–48

[55] Koenders J.T.W., Perek A., Galperti C., Duval B.P., Février O., Theiler C. and Berkel M.V. (the TCV Team) 2023 Systematic design of a multi-input multi-output controller by model-based decoupling: a demonstration on TCV using multi-species gas injection *Nucl. Fusion* **63** 106007

[56] Ravensbergen T. *et al* 2021 Real-time feedback control of the impurity emission front in tokamak divertor plasmas *Nat. Commun.* **12** 1105

[57] Koenders J.T.W., Wensing M., Ravensbergen T., Février O., Perek A. and Berkel M.V. (TCV Team and Eurofusion Team) 2022 Systematic extraction of a control-oriented model from perturbative experiments and SOLPS-ITER for emission front control in TCV *Nucl. Fusion* **62** 066025

[58] Pau A. 2023 A modern framework to support disruption studies: the EUROfusion disruption *Preprint: 2023 IAEA Fusion Energy Conf.* (*London, United Kingdom, 16–21 October 2023*) [EX/P4-21]

[59] Pau A. *et al* 2022 Controlled avoidance of disruptions in tokamaks: experience and developments in TCV *Talk presented at 48th EPS Conf. on Plasma Physics* (*Virtual*, *27 June –1 July 2022*) (available at: https://hdl.handle.net/21.11116/0000-000A-C824-C)

[60] Vu T., Felici F., Galperti C., Maraschek M., Pau A., Rispoli N., Sauter O. and Sieglin B. 2021 Integrated real-time supervisory management for off-normal-event handling and feedback control of tokamak plasmas *IEEE Trans. Nucl. Sci.* **68** 1855–61

[61] Kong M., Felici F., Sauter O., Galperti C., Vu T., Ham C.J., Hender T.C., Maraschek M. and Reich M. (TCV Team, MAST Team, ASDEX Upgrade team, and Eurofusion Team) 2022 Physics-based control of neoclassical tearing modes on TCV *Plasma Phys. Control. Fusion* **64** 044008

[62] Degrave J. *et al* 2022 Magnetic control of tokamak plasmas through deep reinforcement learning *Nature* **602** 414–9

[63] Gorno S. *et al* (the TCV Team) 2024 X-point radiator and power exhaust control in configurations with multiple X-points in TCV *Phys. Plasmas* **31** 072504

[64] Sun G., Reimerdes H., Theiler C., Duval B.P., Carpita M., Colandrea C. and Février O. (the TCV Team) 2023 Performance assessment of a tightly baffled, long-legged divertor configuration in TCV with SOLPS-ITER *Nucl. Fusion* **63** 096011